Energy Conversion and Management 254 (2022) 115277

Contents lists available at ScienceDirect

Energy Conversion and Management

journal homepage: www.elsevier.com/locate/enconman

A study on temperature spatial distribution of a greenhouse under solar load with considering crop transpiration and optical effects

Ke Xu [a,b], Xuan Guo [c], Junming He [d], Bin Yu [e], Jinglu Tan [f], Ya Guo [a,b,*]

[a] Key Laboratory of Advanced Process Control for Light Industry, Ministry of Education, Jiangnan University, Wuxi 214122, China
[b] School of Internet of Things, Jiangnan University, Wuxi 214122, China
[c] College of Civil Science and Engineering, Yangzhou University, Yangzhou 225127, China
[d] Wuxi Kaiyi Internet of Things Technology Development Co. Ltd, Wuxi 214135, China
[e] Jiangsu Nongxing Intelligent Technology Co. Ltd, Wuxi 214028, China
[f] Department of Bioengineering University Missouri, MO 65211, USA

ARTICLE INFO

Keywords:
Temperature distribution
Greenhouse
Energy conservation
Crops transpiration
Computational fluid dynamics

ABSTRACT

Spatial temperature distribution of a greenhouse is critical to precision agriculture management, especially for the vertical cultivation mode. Crop transpiration and optical effects influence spatial temperature distribution of a greenhouse, which, however, were often omitted in literature. In this work, a Computational Fluid Dynamics model on studying spatial temperature distribution of a greenhouse was developed with considering the effects of air (light absorption), crop (light absorption, reflection, transmission, and transpiration), and soil (light absorption and heat radiation) in the greenhouse under dynamic solar load based on the law of energy conservation. A set of field tests was used to validate the developed Computational Fluid Dynamics model. Spatial temperature distributions of the greenhouse under different scenarios were simulated with and without considering crop effects. The results show that the temperature standard deviation of the greenhouse with considering the crop effects was about 31.68% higher than that without considering the crop effects. This implies that greenhouse temperature distribution is significantly influenced by crop transpiration and optical effects. The results also show that the highest temperature appears in the air region below the top of greenhouse and changes with the dynamic solar radiation direction, and the temperature may vary by about 63.65% during the day. There is a temperature difference of 2 °C-3 °C at the same height level between the greenhouse with and without considering the crop effects. This work is important for understanding the non-uniform temperature spatial distribution pattern of a greenhouse as affected by crops, and provides information for sensor deployment, monitoring, and control of greenhouse temperature.

1. Introduction

With the increase of population and the depletion of resources, reducing production cost and energy consumption becomes more and more important [1]. A greenhouse may provide an enclosed space for soil heating/cooling [2], and achieve desirable agriculture production temperature during cold/hot weather conditions [3]. A greenhouse is also applied to dry soil conditions to reduce water consumption [4]. Greenhouse cultivation is an efficient way to increase crop yields [5], and the sustainable development of agriculture production is maintained beneficially [6]. Nowadays, greenhouses have been widely used in agriculture to make environmental conditions as favorable as possible for crop growth [7]. The microclimate in a solar greenhouse is affected by external meteorological conditions, glass types [8], internal components, and crop types, then has an influence on the growth of crops [9].

Temperature is one of the most significant parameters in greenhouse climate. Temperature prediction and control need multifactor modeling based on energy transfer mechanism. Dynamic temperature models [10] of greenhouse air, cover, soil, and wall were established to predict and control of greenhouse temperature [11]. The heat storage material in a greenhouse plays a significant role in raising greenhouse air temperature during cold months [12]. Berroug et al investigated the impact of the phase change material (PCM) on greenhouse temperature, and the results show that the use of north wall made with PCM can increase energy efficiency [13]. In order to improve greenhouse temperature conditions, Sara et al proposed the dynamic analysis of the natural and mechanical ventilation of a solar greenhouse by controlling mechanical ventilation

* Corresponding author.
E-mail address: guoy@jiangnan.edu.cn (Y. Guo).

https://doi.org/10.1016/j.enconman.2022.115277
Received 28 November 2021; Received in revised form 17 January 2022; Accepted 19 January 2022

Nomenclature

a_{air}	Heat radiation absorption coefficient of air (m^{-1})
A_c	Crop transpiration area (m^2)
A_s	Soil evaporation area (m^2)
c_{pa}	Specific heat capacity of air (J kg^{-1} K^{-1})
C_0	Sunny coefficient for solar radiation
E_{ca}	Total crop air energy (J kg^{-1})
E_{cp}	Total crop plant energy (J kg^{-1})
h_{soil_air}	Soil-air convective heat transfer coefficient (W m^{-2} K^{-1})
h_{out_air}	Out-air convective heat transfer coefficient (W m^{-2} K^{-1})
h_{crop_air}	Crop-air convective heat transfer coefficient (W m^{-2} K^{-1})
H_{crop}	Heat flux of crop transpiration (W m^{-2})
H_{soil}	Heat flux of soil evaporation (W m^{-2})
I_{air}	Radiation intensity, which depends on location ($\vec{r}$) and direction ($\vec{s}$)
k_{air}	Air thermal conductivity (W m^{-1} K^{-1})
k_{ca}	Air thermal conductivity of crops (W m^{-1} K^{-1})
k_{cp}	Thermal conductivity of crops (W m^{-1} K^{-1})
k_{crop}	Effective thermal conductivity of crops (W m^{-1} K^{-1})
k_{soil}	Soil thermal conductivity (W m^{-1} K^{-1})
n	Direction vector perpendicular to the boundary
n_{air}	Air refractive index
p_{air}	Air pressure (pa)
R_{bd}	Irradiance at the boundary (W m^{-2})
R_{crop}	Crop heat radiation (W m^{-2})
R_{dir}	Direct normal solar radiation (W m^{-2})
R_{dif}	Diffuse solar radiation (W m^{-2})
R_{solar}	Total solar irradiance (W m^{-2})
R_{soil}	Soil heat radiation (W m^{-2})
R_{sc}	Solar radiation reaching the surface of crops (W m^{-2})
R_{ss}	Solar radiation reaching the surface of soil (W m^{-2})
S_a	Energy source term of absorbed heat radiation per unit volume of air (W m^{-3})
S_{by}	Buoyancy source term of air (kg m^{-2} s^{-2})
S_{et}	Energy source term of evapotranspiration per unit volume of air (W m^{-3})
t	Local real time (s)
T_{air}	Air temperature (K)
T_{crop}	Crop temperature(K)
T_{out}	Outside air temperature (K)
T_{ref}	Reference temperature (K)
T_{soil}	Soil temperature (K)
u_{ia}	Air flow velocity (m s^{-1})
u_{vent}	Vent velocity (m s^{-1})
V_{air}	Greenhouse air volume (m^3)
x_i	Three-dimensional location component (m)

Greek symbols

α_{crop}	Solar radiation absorption rate of crops
α_{soil}	Solar radiation absorption rate of soil
β_{air}	Coefficient of thermal expansion (K^{-1})
γ_c	Crop porosity
ρ_{air}	Air density (kg m^{-3})
ρ_{ca}	Air density in crop area (kg m^{-3})
ρ_{cp}	Plant density in crop area (kg m^{-3})
ρ_{ref}	Reference density (kg m^{-3})
μ	Dynamic viscosity (kg m^{-1} s^{-1})
σ	Stefan-Boltzmann constant (W m^{-2} K^{-4})
η_{crop}	Light transmittance of crops
η_f	Light transmittance of greenhouse film
ε_{crop}	Crop thermal emissivity
ε_{soil}	Soil thermal emissivity
Ω	Radiant solid angle (sr)
Φ	Phase function

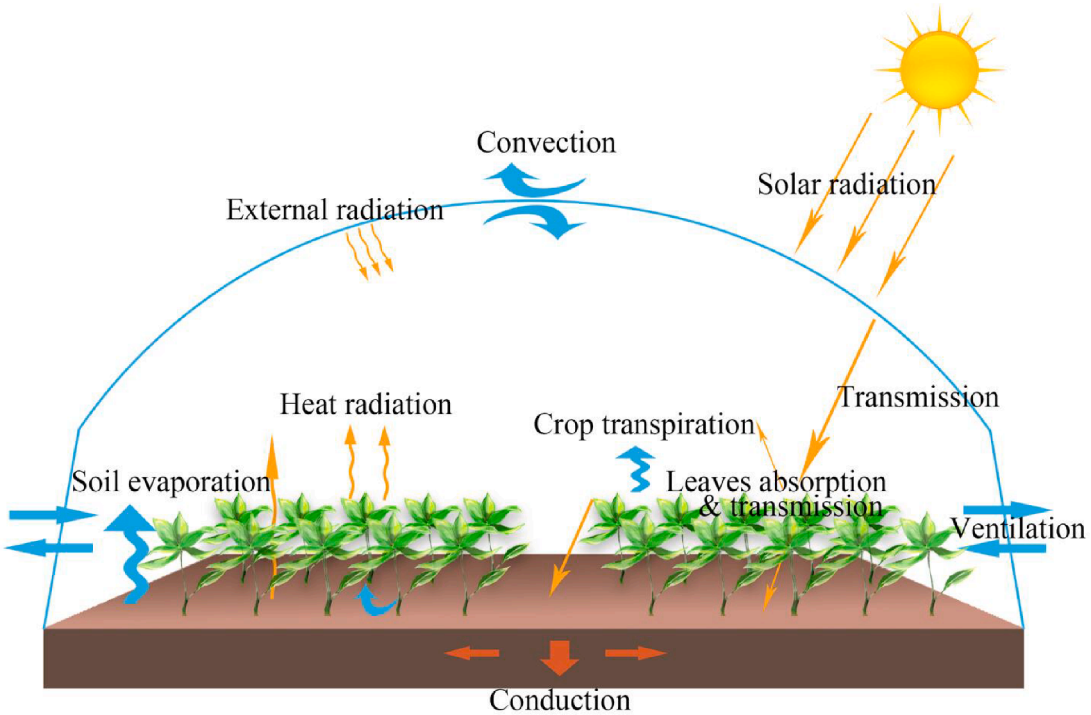

Fig. 1. A schematic diagram of energy conversion inside a greenhouse.

with an Earth-to-Air Heat Exchanger [14]. However, due to differences in boundary conditions and material properties [15], the temperature distribution of a greenhouse is always complicated [16]. Cristina et al proposed a reference methodology of greenhouse dynamic simulation to assess crop thermal well-being and energy needs [17]. Soil surface conditions also affect greenhouse temperatures, in order to study the thermal effect of soil surface mulch, Francisco et al established a greenhouse energy model that takes into account soil layers covered in polypropylene [18]. Serageldin et al investigated the thermal performance of an Earth-Air Heat Exchanger used for heating and cooling purposes under Egyptian weather conditions [19].

Uneven temperature distribution may lead to the uneven growth status of crops at different locations, resulting in difficulty in greenhouse production management. For more accurate management of greenhouse planting environment, Computational Fluid Dynamics (CFD) [20] was used to analyze the spatial heterogeneity of greenhouse temperature distribution under the influence of various factors [21]. Saberian et al developed a CFD model of an empty greenhouse with considering the influence of dynamic solar radiation on the internal temperature of the greenhouse to predict the dynamic greenhouse temperature distribution, and evaluated the effect of ventilation on heat dissipation of greenhouse in summer [22].

Crops may affect greenhouse temperature spatial distribution non-uniformly. This brings difficulty in understanding the microclimate in a greenhouse and temperature sensor deployment, monitoring, and control. The objective of the study was to comprehensively analyze greenhouse temperature distribution mechanism with considering effects of crop transpiration and optical effects under dynamic solar radiation, and provide information for greenhouse temperature sensor deployment and temperature management. A CFD model of greenhouse temperature distribution was established in this work with and without considering crop effects.

2. Methods

A mathematical model of energy conversion in a greenhouse based on the law of energy balance was developed, and the temperature distribution data of agricultural solar greenhouse was measured by sensors. Finally, the temperature distribution of the greenhouse affected by crop transpiration and optical effects was analyzed through the ANSYS-Fluent software.

2.1. Greenhouse energy conversion model

The microclimate of a greenhouse is a dynamic nonlinear system with strong coupling of multiple factors [23]. The dynamic solar radiation shines on crop leaves and soil surface through the translucent greenhouse film. Soil and crops convert energy through transpiration and evaporation. Detailed energy conversion process of a greenhouse is illustrated in Fig. 1.

In order to consider the effect of evapotranspiration on greenhouse energy, the latent heat energy from soil evaporation and crop transpiration, and the absorption effect of radiation by the wet air in the greenhouse, were included in the air energy model.

$$\rho_{air}c_{pa}\frac{\partial T_{air}}{\partial t}+\rho_{air}c_{pa}u_{ia}\frac{\partial T_{air}}{\partial x_i}=k_{air}\frac{\partial^2 T_{air}}{\partial x_i^2}+S_{et}+S_a \tag{1}$$

Here ρ_{air} is the air density, c_{pa} is the air specific heat capacity, T_{air} is the air temperature, u_{ia} is the air flow rate, k_{air} is the air thermal conductivity, k_{air} is the air thermal conductivity, and x_i is the three-dimensional location component. The sources term S_{et} in Eq. (1) is the energy input per unit volume of soil evaporation and crop transpiration source term, which is calculated as Eq. (2).

$$S_{et} = \left(\frac{A_c H_{crop}+A_s H_{soil}}{V_{air}}\right) \tag{2}$$

Here A_c and A_s are the surface areas of crop transpiration and soil evaporation, respectively. H_{crop} and H_{soil} are the latent heat flux densities of crop transpiration and soil evaporation input, respectively, which can be calculated through the Shuttleworth-Wallace dual-source model [24].

$$H_{crop}=\lambda_w W_{crop}=C_c\frac{\Delta R^{'}+\left(\left(\rho_{air}c_{pa}D-\Delta r_a^c R_s^{'}\right)/\left(r_a^a+r_a^c\right)\right)}{\Delta+\gamma\left(1+\left(r_s^c/\left(r_a^a+r_a^c\right)\right)\right)} \tag{3}$$

$$H_{soil}=\lambda_w W_{soil}=C_s\frac{\Delta R^{'}+\left(\left(\rho_{air}c_{pa}D-\Delta r_a^c\left(R^{'}-R_s^{'}\right)\right)/\left(r_a^a+r_a^c\right)\right)}{\Delta+\gamma\left(1+\left(r_s^s/\left(r_a^a+r_a^s\right)\right)\right)} \tag{4}$$

Here λ_w is the latent heat of vaporization of water, W_{crop} and W_{soil} are evapotranspiration of crops and soil, respectively. C_c and C_s are aerodynamic resistance coefficients of crop canopy and soil surface, respectively. $R^{'}$ and $R_s^{'}$ are the available energy leaving from the canopy and soil surface, respectively. r_a^a is aerodynamic resistance between mean canopy flow and reference height, r_a^c is canopy boundary resistance, r_a^s is aerodynamic resistance between soil surface and mean canopy flow, r_s^c is canopy stomatal resistance, r_s^s is soil surface evaporation resistance, Δ is the slope of the vapor pressure temperature curve, and D is the saturated vapor pressure.

S_a in Eq. (1) is the energy absorbed by the wet air as a unit volume source term in the air energy equation, and the integration operation is performed over the control volume for the radiation intensity.

$$S_a=a_{air}\int_0^{4\pi} I_{air}(\vec{r},\vec{s})\Omega d\Omega \tag{5}$$

Here I_{air} is the radiation intensity in the air, a_{air} is the air absorption coefficient of heat radiation, Ω is the radiation stereo angle. In order to consider the air absorption of radiation, the discrete coordinate (DO) radiation model [15] was used in this work. The model covers the entire optical thickness and can be coupled with the energy equation to calculate the energy distribution of the discrete radiation field. The model is described by the radiation intensity transfer model as Eq. (6).

$$\begin{aligned}&\frac{\partial(I_{air}(\vec{r},\vec{s})\vec{s})}{\partial x_i}+(a_{air}+\sigma_s)I_{air}(\vec{r},\vec{s})\\&=a_{air}n_{air}^2\frac{\sigma T_{air}^4}{\pi}+\frac{\sigma_s}{4\pi}\int_0^{4\pi} I_{air}(\vec{r},\vec{s}^{\,'})\Phi(\vec{s}\cdot\vec{s}^{\,'})d\Omega\end{aligned} \tag{6}$$

Here r and s are the location vector and direction vector, respectively. n_{air} is the refractive index of the participating medium, σ is the Stephan-Boltzmann constant (5.67×10^{-8} W m^{-2} K^{-4}), σ_s is the light scattering coefficient of air medium, and Φ is the phase function. The relationship between radiation intensity and irradiance R_{bd} at the boundary is described as Eq. (7).

$$R_{bd}=\int_0^{4\pi} I_{air}(\vec{r},\vec{s})\Omega d\Omega \tag{7}$$

At the boundary of the greenhouse film, R_{solar} is the amount of radiation from by the sun and the outside environment through the greenhouse film.

$$R_{solar}=C_0\eta_f\left(R_{dir}+R_{dif}\right) \tag{8}$$

Here C_0 is the sunny coefficient, η_f is the transmittance of the greenhouse film. R_{dir} and R_{dif} are direct and diffuse radiation from the sun and the outside of the greenhouse, and can be calculated according to the ASHRAE (American Society of Heating, Refrigerating and Air-Conditioning Engineers) model [25]. The ASHRAE model needs the input information of latitude, longitude, time zone, and the geographic direction. Model details are listed in Appendix A. The radiation boundary of soil and crop canopy may be calculated as follows.

$$R_{soil}=(1-\alpha_{soil})R_{ss}+n_{air}^2\varepsilon_{soil}\sigma T_{soil}^4 \tag{9}$$

Fig. 2. Actual conditions inside the greenhouse.

$$R_{crop} = \left(1 - \alpha_{crop} - \eta_{crop}\right)R_{sc} + n_{air}^2 \varepsilon_{crop}\sigma T_{crop}^4 \tag{10}$$

Here α_{soil} and α_{crop} are the heat radiation absorption rate of soil surface and crop leaves, respectively. ε_{soil} and ε_{crop} are the radiation emission rate of soil surface and crop leaves, respectively. η_{crop} is the light transmission rate of crop leaves. R_{ss} and R_{sc} are the solar radiation reaching soil surface and crop surface, respectively. The convective heat transfer at the boundary of the film is shown in Eq. (11).

$$k_{air}\frac{\partial T_{air}}{\partial n} = h_{out\_air}(T_{out} - T_{air}) \tag{11}$$

Here h_{out_air} is the convective heat transfer coefficients of the film and air. T_{out} is the outside temperature.

In the crop area, the liquid water is converted into water vapor of air through transpiration, and the sensible heat of leaves is converted into latent heat of water vapor. The crop area was considered as a porous medium material in this study as done in [15]. The equilibrium thermal model of crops is shown in Eq. (12).

$$\frac{\partial}{\partial t}\left(\gamma_c \rho_{ca} E_{ca} + (1-\gamma_c)\rho_{cp}E_{cp}\right) + \frac{\partial}{\partial x_i}\left(u_{ic}(\rho_{ca}E_{ca} + p_c)\right) = k_{crop}\frac{\partial^2 T_{crop}}{\partial x_i^2} \tag{12}$$

$$k_{crop} = \gamma_c k_{ca} + (1-\gamma_c)k_{cp} \tag{13}$$

Here γ_c is the porosity of the crop area, ρ_{ca} and ρ_{cp} are the air density and plant branch density, respectively. E_{ca} and E_{cp} are the total energy of air and solid media, respectively. u_{ic} is the air velocity of the crop area, k_{crop} is the effective thermal conductivity of the crop media. k_{ca} and k_{cp} are the thermal conductivity of air and plant media, respectively. On the interface between crops and air, the canopy leaves carry out convective heat dissipation, absorb solar radiation, and produce thermal radiation. At the contact surface with the soil, $T_{crop} = T_{soil}$.

$$k_{crop}\frac{\partial T_{crop}}{\partial n} = \alpha_{crop}R_{sc} + h_{crop\_air}\left(T_{air} - T_{crop}\right) - \varepsilon_{crop}\sigma T_{crop}^4 - H_{crop} \tag{14}$$

Some solar radiation is absorbed by exposed soil surface. Then soil convective heat exchanges with air and releases thermal radiation to the air domain, and loses some energy through evaporation.

$$-k_{soil}\frac{\partial T_{soil}}{\partial y} = \alpha_{soil}R_{ss} + h_{soil\_air}(T_{air} - T_{soil}) - \varepsilon_{soil}\sigma T_{soil}^4 - H_{soil} \tag{15}$$

Here k_{soil} is soil thermal conductivity.

In order to consider the influence of the flow state of greenhouse air on temperature distribution, the Navier-Stokes equations can be used and the buoyancy effect is introduced as a source or sink of momentum in the momentum equation. The Boussinesq approximation was used with air density [20]. And the standard k-ε two-equation turbulence model [26] was applied in this study. The turbulence model is shown in Appendix B. The velocity equations of the air are listed according to the law of momentum conservation as follows:

$$\rho_{air}\frac{\partial u_{ia}}{\partial t} + \rho_{air}u_{ia}\frac{\partial u_{ia}}{\partial x_i} = -\frac{\partial p_{air}}{\partial x_i} + S_{by} \tag{16}$$

$$S_{by} = \rho_{ref}g\left(1 - \beta_{air}\left(T_{air} - T_{ref}\right)\right) \tag{17}$$

Here S_{by} in Eq. (16) is the buoyancy effect due to the thermal expansion of air, p_{air} is the air pressure, ρ_{ref} is the reference density, β_{air} is the coefficient of thermal expansion of air, and T_{ref} is the reference temperature.

2.2. Experimental measurement

In order to verify the performance of the CFD model, experiments were conducted from a greenhouse (with 8 m span, 3.3 m ridge height, 1.8 m vent height, 60 m length) on September 27, 2021 with sunny sky. It is a south-north oriented single plastic (polyethylene film) greenhouse arc-shaped top structure (Fig. 2) locating in Zhuqiao Town, Pudong New Area, Shanghai, 121.78 E, 31.09 N. During measurement, cucumbers with vines of 1.5 m in height were growing in the greenhouse. It was with natural ventilation on the east and west sides, and the cucumbers were planted east–west.

In order to monitor the temperature inside the greenhouse, sensors from Shandong Renke Measurement and Control Technology Company were ordered. Air temperature sensors (COS-04-X USB type) were employed, which can record 80,000 temperature data. The measurement range of the air temperature sensors is −20 °C~ +60 °C, the measurement accuracy is ± 0.3 °C (25 °C), and the resolution is 0.1 °C. The soil temperature sensors (RS-WS-N01-TR-1 type) were set to monitor the temperature of crop-covered soil and exposed soil, respectively. A crop leaf temperature sensor (PR-3001-YM-*-N01 type) was set to measure temperature of crops canopy. Both soil temperature sensor and leaf temperature sensor are with a measurement range of −40 °C~ +80 °C, measurement accuracy of ± 0.5 °C (25 °C) and resolution of 0.1 °C. They are connected to the data logger (RS-REC-USBN01-1 type) for data storage through RS485 as shown in Fig. 3. The T1-T10 temperature

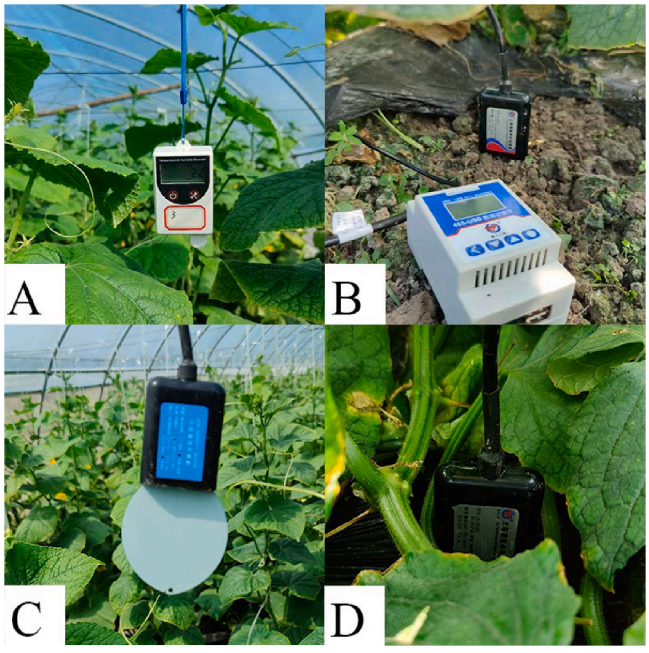

Fig. 3. A picture of sensor and device deployment. A-air temperature sensor, B-temperature logger, C-leaf temperature sensor, and D-soil temperature sensor.

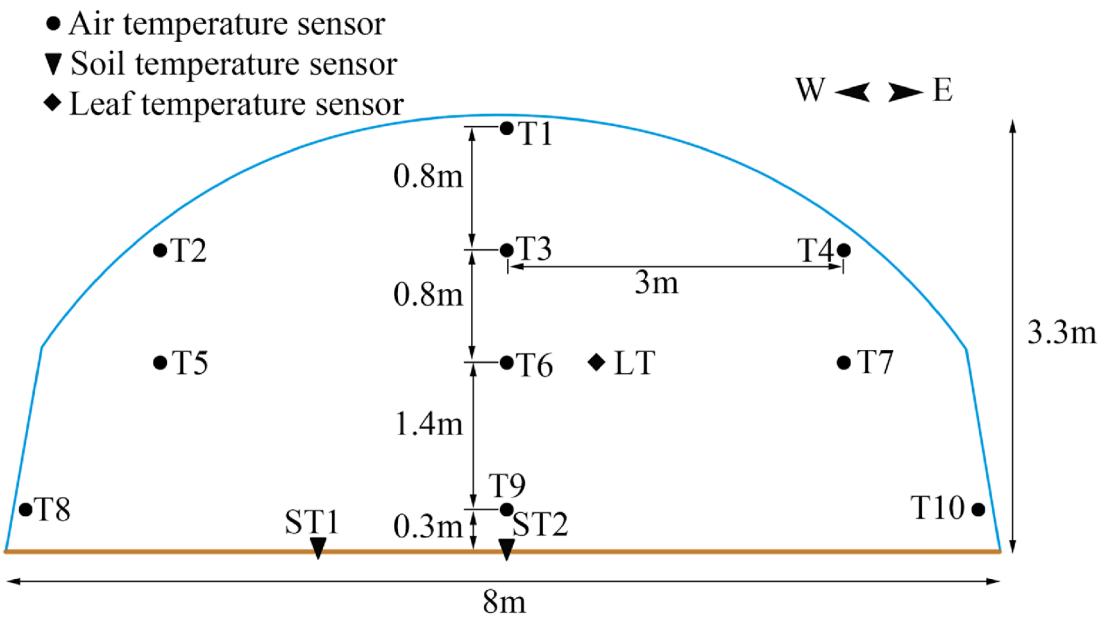

Fig. 4. Deployment of temperature sensors in the middle radial section of the greenhouse.

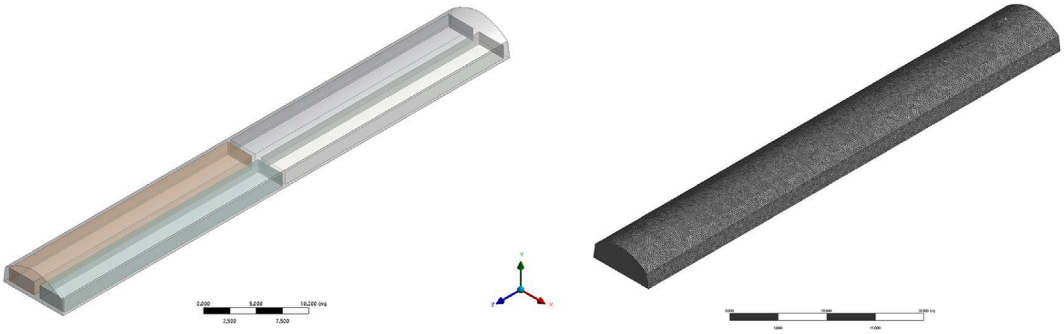

Fig. 5. The left side of the figure shows the physical model, and the right side shows the meshing.

Table 1
Material thermal properties.

Material	Density (kg m^{-2})	Specific Heat (J kg^{-1} K^{-1})	Thermal Conductivity (W m^{-1} K^{-1})	Dynamic Viscosity (kg m^{-1} s^{-1})	Thermal Expansion Coefficient(K^{-1})
Air	1.225	1006.43	2.42×10^{-2}	1.789×10^{-5}	3.43×10^{-3}
Crop	800	3000	20	–	–
Polyethylene	920	2300	0.34	–	–
Soil	2200	2500	1.5	–	–

sensors were placed at a cross section of the greenhouse. All the sensors were deployed at four layers in the vertical direction. The sensor deployment details of the temperature sensors are shown in Fig. 4. The temperature sensors measured continuously throughout the day and the data recording time interval was set as 2 minutes.

Table 2
Optical properties of materials.

Material/ Location	Absorption coefficient (m^{-1})	Emissivity	Absorptivity	Transmissivity
Air	0.20	–	–	–
film	–	0.92	0.10	0.80
crop leaves	–	0.85	0.02	0.50
Soil	–	0.89	0.50	–

2.3. Numerical simulation settings

In order to analyze the greenhouse temperature field more accurately, the experimental greenhouse was modeled and numerically calculated in 1:1 ratio. The geometric model of the greenhouse was established by the ANSYS Design Model module. The automatic meshing method in ANSYS Meshing was used to divide the computational domain grids. The grid element size was set as 0.18 m. There were 247,587 nodes with 865,647 units. The average mesh quality is 0.85222, which is greater than the minimum mesh quality requirement of 0.7. The average mesh skewness is 0.20486, which is well below 0.9 and satisfies requirement. Geometric modeling and meshing are shown in Fig. 5.

The numerical solution was performed using the computational fluid dynamics software ANSYS Fluent 2021R1 in this study. The finite volume method was used to solve the computational domain. In this study, in order to consider the flow condition of greenhouse air, the standard *k*-

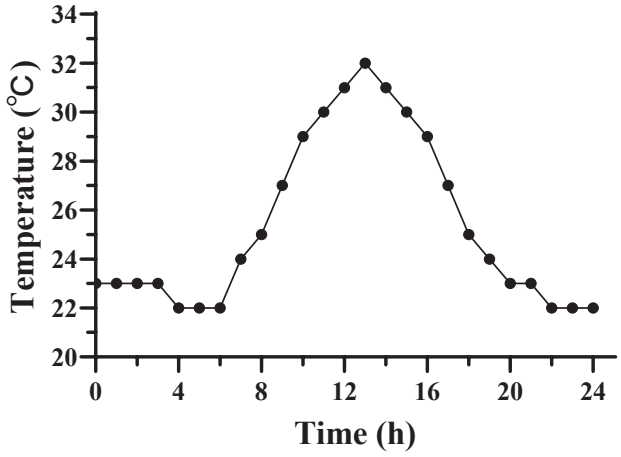

Fig. 6. External air temperature.

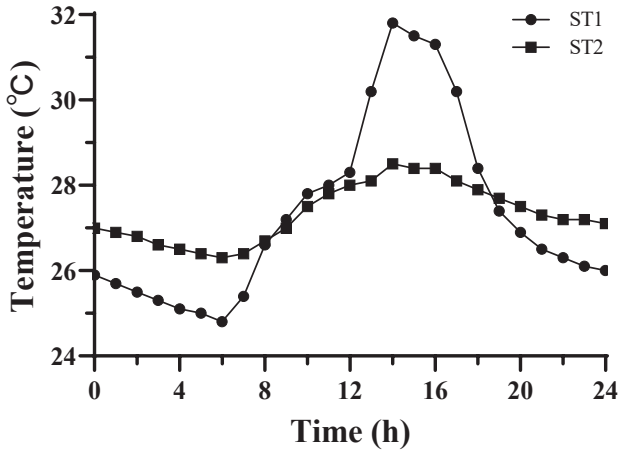

Fig.7. Temperature changes over the day in bare soil and soil under plant cover measured with ST1 and ST2, respectively.

Table 3
Boundary conditions.

Location	Boundary Conditions
South side film, roof film	Heat transfer coefficient: 4 W/m^2 K. External convection temperature was obtained from meteorological temperature (Fig. 6). Radiation: 'Use beam direction from solar load model settings' and 'Use irradiation from solar load model settings' were selected in the menu bar of Fluent software
East side film, west side film	Imposed external weather temperature, Radiation: Solar load model setting
North side film	Imposed external weather temperature
Crop leaves	Coupled wall
Covered soil	Imposed temperature: 28 °C, Internal Emissivity: 0.9
Exposed soil	Mixed: Heat transfer coefficient: 1.5 W/m^2 K. External convection temperature: 30 °C

ε turbulence model was employed as done in [27]. To consider the absorption of solar radiation by air, the DO radiation model and solar irradiation model were used. The model material thermal properties were set as constants in Table 1 according to relevant works [15,16].

The greenhouse film and crop leaves were treated as semi-transparent boundary, and the soil was treated as opaque boundary. The surface absorptivity and transmissivity of radiation were set as Table 2. Optical properties of different materials were set as constants within a reasonable range according to the references [16,28,29].

Setting the radiation boundary of the greenhouse film needs to consider the influence of environmental radiation. 25 °C was set as the environmental base temperature in the early morning according to experimental data, and the solar radiation factor was adjusted to make simulations match measured temperature time series, which was determined as 0.2 in this work. The latent heat of crop transpiration is 2260 kJ/kg. The temperature boundary conditions and initial conditions of the greenhouse were set according to the experimental temperature measurement. The greenhouse film convection boundary was set as the outdoor air temperature, which is shown in the Fig. 6. The temperature of the exposed soil surface denoted as ST1 and the soil temperature covered by crops denoted as ST2 were shown in Fig. 7. Details of the boundary settings were shown in Table 3.

The pressure-based solver and the SIMPLEC solver algorithm were used to accelerate convergence. The second-order upwind format discrete method was used with default pressure, density, momentum, and k-ε sub-relaxation factors. The iteration number of the calculation process was set as 1000. The results were saved and presented by the CFD-POST post-processing software. In order to investigate the effect of crops on greenhouse temperature distribution, comparative simulations were conducted with and without considering crops in this study. A set of steady-state simulations were both carried out in a two-hour time step, and the numerical simulation results at the cross section of 9: 00, 11: 00, 13: 00, and 15: 00 were obtained. Computer CPU unit is Intel Xeon CPU E5-1620. Computer main frequency is 3.50 GHz with 4 cores and 8 threads. RAM of the computer is 64 GB. In this study, double precision and 8 threads were applied for high-speed calculation.

3. Results and discussion

In this section, the simulated data were compared with measured data to verify the CFD model's performance on greenhouse temperature simulation. And the differences in comparison of simulation results with and without considering the effects of crops was shown. The influence of crop transpiration and optical effects on the spatial distribution of greenhouse temperature was discussed.

3.1. Verification of the developed model

The measured temperature data of 9:00, 11:00, 13:00 and 15:00 for the sensor layout in Fig. 4 is shown in Fig. 8, and the simulated temperature distribution is shown in Fig. 9.

The average deviation between simulated temperature (at location of temperature sensors) and measured temperature (T1-T10 temperature sensors) at 9:00, 11:00, 13:00, and 15:00 was 4.62 %, 5.09 %, 7.69 %, and 5.38 % respectively. The simulated temperature and measured temperature of the crop canopy are shown in Fig. 10, with 4.75 % average deviation. It can be seen that the temperature deviations at different times are within a reasonable range, which proved the effectiveness of the CFD numerical simulations.

The temperature of crop leaves increased rapidly with the duration of solar radiation. When the temperature reached about 40 °C, the temperature does not continuously rise, which might be explained by the transpiration of crops taking away a lot of energy. It also can be seen that both simulation and measurement of greenhouse temperature change with time and space. The greenhouse temperature is distributed regionally and hierarchically with obvious differences. The high-temperature region in the greenhouse changes with the solar radiation direction.

To show the regularity of temperature distribution vertically, the temperature data of temperature sensors of T1, T3, and T6 under dynamic solar radiation are shown in Fig. 11. It can be seen that the temperature gradually rises about 12 °C-18 °C from 7:00 to 11:00. The temperature goes down between 11:00 and 13:00 (temperature sampling interval is 2 h as stated in the experiments section). The temperature drops gradually from top to bottom, and the temperature

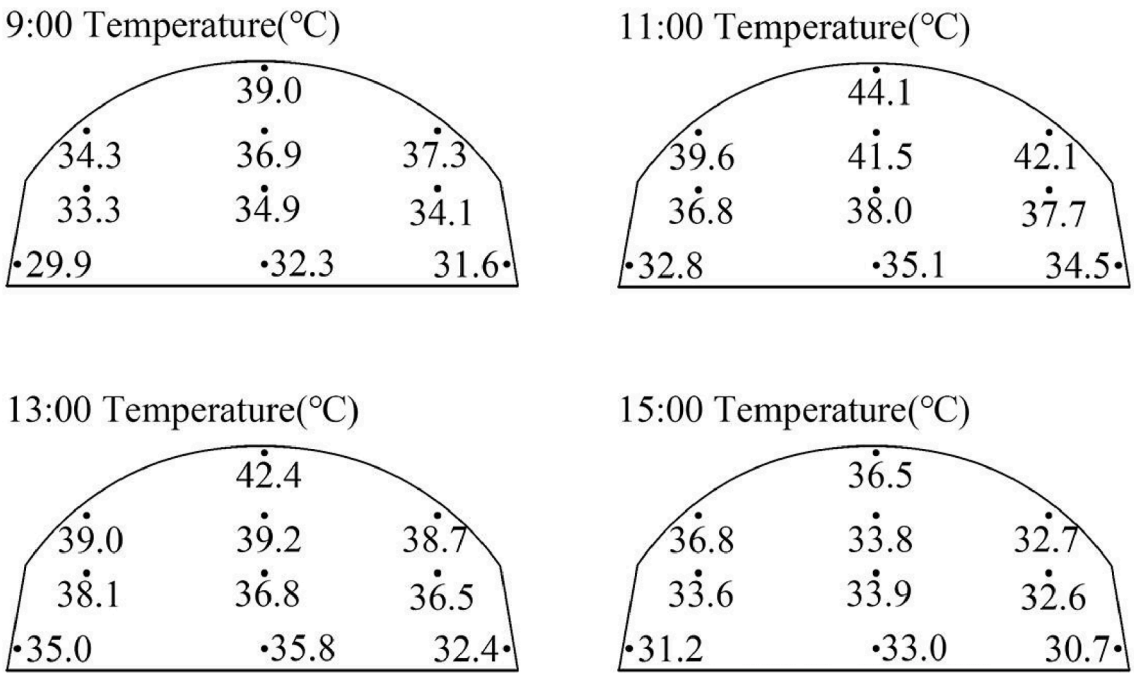

Fig. 8. Measured temperature distribution in the middle cross section of greenhouse with considering the effects of crops from 9:00–15:00.

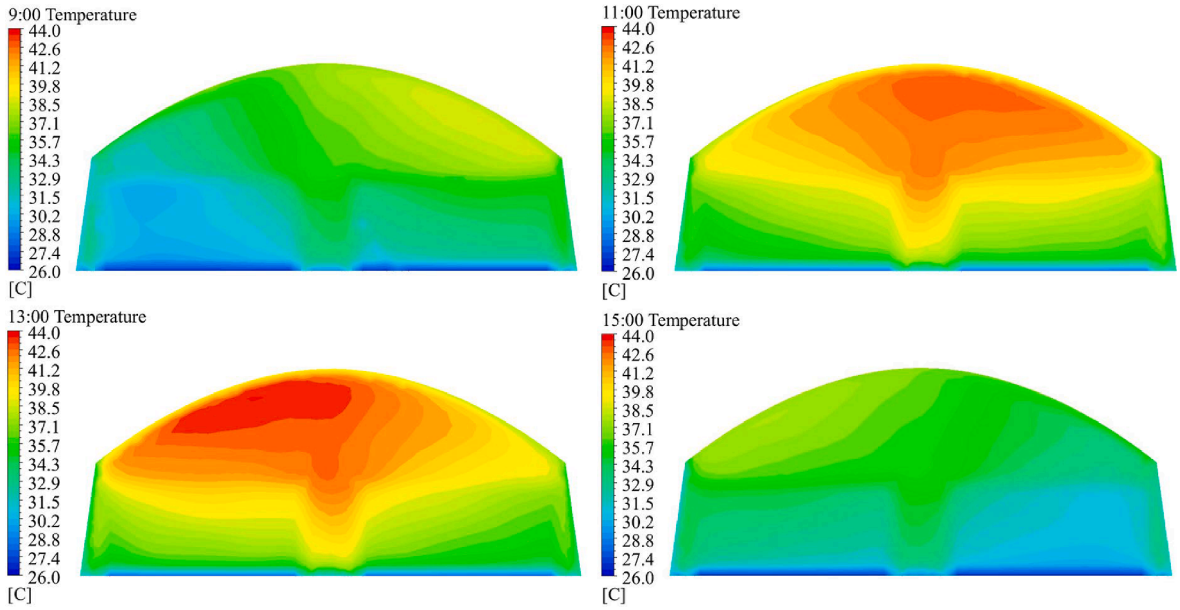

Fig. 9. Simulated temperature distribution in the middle cross section of greenhouse with considering the effects of crops from 9:00–15:00.

difference at different heights is the largest during the midday hours, but there is little temperature difference between morning and evening.

3.2. Comparison of simulations with and without considering the effects of crops

Simulations with and without considering the effects of crops are shown in Figure are shown in Fig. 9 and Fig. 12, respectively. It can be seen that higher air temperature distribution above the crops is more uniform than that without considering the crop effects as shown in Fig. 9, the temperature at the location of crop areas is lower than the temperature at the corresponding location of the greenhouse without considering the crop effects (Fig. 12). And the air temperature above the middle road is higher than the temperature at the location of crop areas, which leads to the formation of downward-curving isotherms above the road when the crop effects are considered (Fig. 9). In the simulations without considering the crop effects, the gradation of greenhouse temperatures is more uniform compared with the temperature distribution with considering the crop effects, although the temperature gradually decreases from top to bottom. The air temperature without considering the crop effects is generally lower than that in the greenhouse with considering crops. And the air temperature without considering the crop effects is higher than the temperature near the soil surface below the crops when the crop effects are considered.

In the comparative simulation without considering the crops effects, the high temperature area inside the greenhouse also appears right

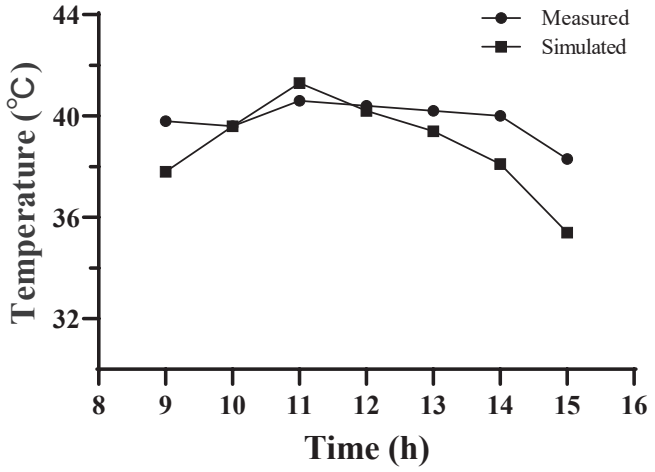

Fig. 10. Simulated temperature and measured temperature of crop canopy.

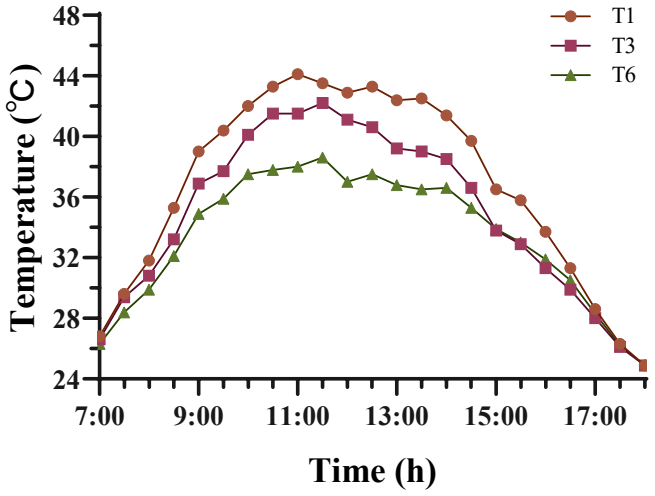

Fig. 11. Temperature measurements at different altitudes throughout the day.

under the greenhouse film, and its location changes with sunlight radiation direction as shown in Fig. 12. The volume of the high temperature area inside the greenhouse without considering the crop effects is larger than that with considering the crop effects during the time of 11:00–13:00. The simulation results show that the temperature extreme differences are 12.0 °C, 15.1 °C, 15.6 °C, and 10.7 °C in the greenhouse with considering the crop effects, and are 8.0 °C, 13.4 °C, 12.2 °C, and 8.3 °C at 9:00, 11:00, 13:00 and 15:00 in the greenhouse without considering the crop effects. It can be seen that the temperature difference between different locations at noon is higher than that in the morning and in the afternoon, and the temperature difference in the greenhouse with considering the crop effects is higher than that without considering crops. The temperature of vertical distribution in other times also shows that temperature value increases from bottom to top. The high-temperature area moves from east to west during a daytime, as shown in Figs. 9 and 12. In order to show the horizontal temperature distribution of the greenhouse, the vertical view of greenhouse temperature is shown in Appendix C.

In order to analyze the spatial distribution of the greenhouse

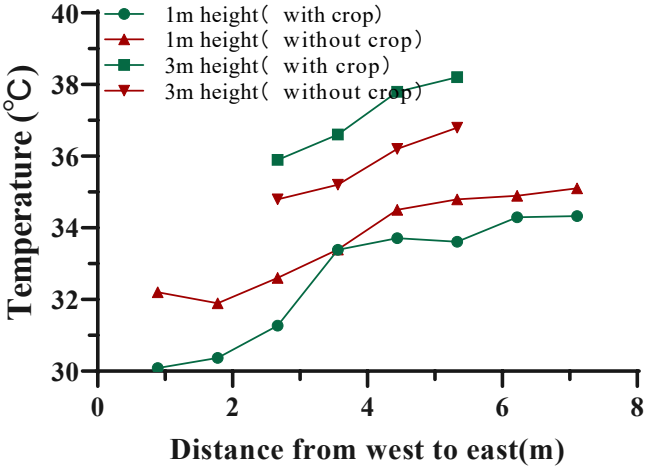

Fig. 13. Horizontal temperature distribution at the cross section of greenhouse at 9:00.

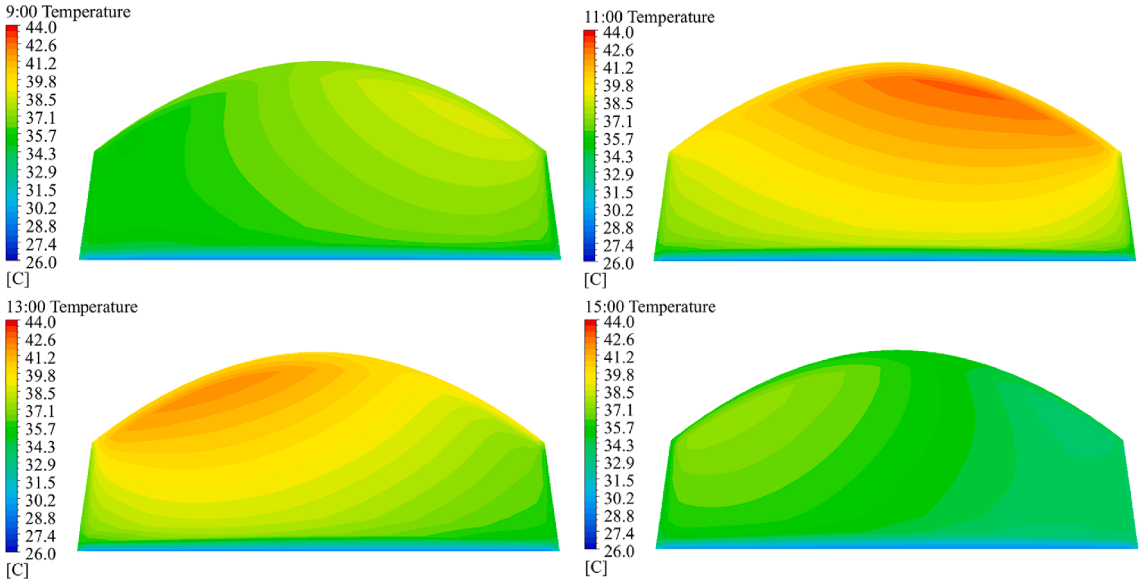

Fig. 12. Simulation of temperature distribution of greenhouse at the moment of 9:00–15:00 without considering the crop model.

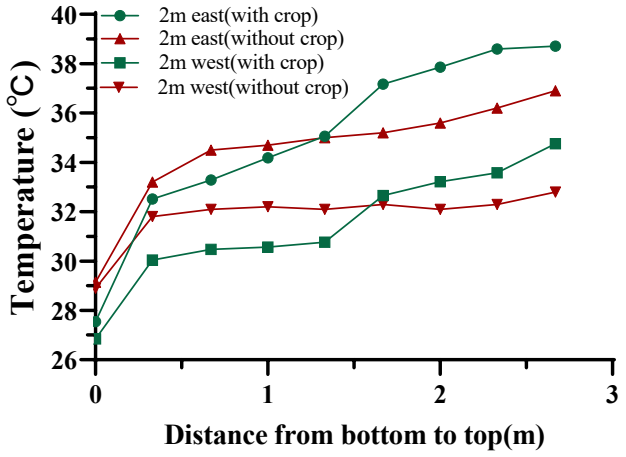

Fig. 14. Vertical temperature distribution at the cross section of greenhouse at 9:00.

temperature (with considering crop and without considering crop), the horizontal location with a height of 1 m and 3 m, and the vertical location 2 m away from the east and west sides, were selected for comparison in this work. As shown in Fig. 13, the temperature gradually rises from west to east in the horizontal direction, and the temperature of the greenhouse with considering the crop effects is about 1 °C lower (2 °C higher) than the greenhouse without considering the crop effects at 1 m (3 m) height. As shown in Fig. 14, the temperature gradually rises from bottom to top in the vertical direction, it also can be seen that the temperature below 1.5 m height without considering the crop effects is 2 °C-3 °C higher than that in the crop area of the greenhouse, and the air temperature above 1.5 m height without considering the crop effects is 2 °C-3 °C lower than that in greenhouse with considering the crop effects.

The height of the crop area is 1.5 m, and the 1.5 m-3.3 m height of the greenhouse is the air area in this study. Solar radiation is the same for the greenhouse with or without considering the crop effects. In the empty greenhouse, most of solar energy is absorbed by soil, which has a very strong heat storage capacity. However, in the greenhouse with considering the crop effects, less solar radiation reaches the soil because of crop canopy, and most of the solar energy is absorbed and reflected by the crops, and the absorbed energy is re-emitted into the air region of the greenhouse. Crops impede air and temperature circulation close to the ground level. This makes crops affect temperature space distribution nonuniformly and results in that the temperature of the crop area below 1.5 m was lower than that of the empty greenhouse, and the air area above 1.5 m was higher than that of the empty greenhouse (Figs. 13 and 14).

Furthermore, in order to evaluate the greenhouse temperature dispersion, the standard deviation was calculated according to Eq. (18).

$$\sigma = \sqrt{\frac{\sum_{t=0}^{n}(T - T_0)^2}{n}} \tag{18}$$

Here σ is the standard deviation of greenhouse temperature. T_0 is the average temperature at the interface. The standard deviation represents the degree of dispersion of the temperature data. A lower standard deviation represents the temperature data are relatively more concentrated, which imply better uniformity. The calculated results at 9:00, 11:00, 13:00, and 15:00 are shown in Table 4.

Table 4
The standard deviation of greenhouse temperature at the cross section.

Standard deviation	With considering the crop effects	Without considering the crop effects
9:00	2.40	1.13
11:00	2.23	1.76
13:00	2.21	1.81
15:00	1.79	1.17

From Table 4, it can be seen that the standard deviation of the greenhouse temperature distribution without considering the crop effects was about 31.68 % lower than that with considering the crop effects. This implies that the uniformity of greenhouse temperature changes when considering crop influence.

3.3. Discussion

The results of this study show the spatial distribution and uniformity of greenhouse temperature are affected by crop evaporation and optical effects. In the energy conversion process of crops and soil, most of the short-wave radiation of the sun is changed into long-wave radiation that cannot pass through the greenhouse film, which is consistent with [28]. And the latent and sensible heat of crops play an important role in greenhouse microclimate energy flux distribution, which is similar to the study in [30]. The greenhouse temperature distribution is the overall effects of external meteorological factors and internal crop energy conversion. It is thus not sufficient to directly attribute the distribution of greenhouse temperature to the conduction of high and low temperature regions in an empty greenhouse as done in literature [22].

The simulation results indicate that temperature has a large difference in the space distribution of the greenhouse. This information is important for temperature sensor deployment and temperature interpretation in a greenhouse especially for temperature monitoring and control. Different crops have different environmental need for growth. Enlightened by this work, more simulations can be performed for a stereoscopic greenhouse. In this way, spatial temperature nonuniform distribution of a stereoscopic greenhouse can be determined. This will allow planting different varieties of crops at different levels of height to make better use of natural temperature distribution nonuniformity and reduce carbon emission.

Although the distribution of the greenhouse temperature with considering the crops effects was analyzed in this study, greenhouse ventilation with considering air flow resistance from crops, the distribution of CO_2 (Carbon dioxide) concentration with considering crop photosynthesis and respiration, and humidity distribution in a greenhouse also can be studied in the future. In this study, the material parameters were set as a constant in this work, but the shape and size of the greenhouse, variety of crop, moisture and color of soil, and many other factors are not fixed. Therefore, different greenhouse environments may be analyzed with considering different attributes. The instantaneous strong ventilation is unpredictable, and its instantaneous impact on greenhouse temperature was ignored in this work, which may also produce certain errors. The solar spectral range was not considered in this study. Because the energy conversion rate of solar spectrum in different bands is different inside the greenhouse, this may be completed in future research.

4. Conclusion

The study aims to analyze the temperature spatial distribution of a solar greenhouse under the coupled effects of external meteorological environment and internal crops. Based on the energy conversion mechanism, a greenhouse multi-factor coupling energy balance model considering crop transpiration and optical effects was established and simulated. The results show that the highest temperature region below the top of the greenhouse changes with the direction of solar radiation, and the temperature first increases and then decreases with the dynamic solar radiation from morning to afternoon. There is a temperature difference of 2 °C-3 °C at the same height level between the greenhouse with considering and without considering the crop effects, and the

temperature uniformity of greenhouse with considering the crop effects is 31.68 % lower than that without considering the crop effects. It can be seen that crops play an important role in greenhouse energy conversion and influence temperature distribution. The results unveil the mechanism of the nonuniform microclimate formation, and provide useful information for temperature sensor deployment and temperature interpretation in a greenhouse, and are important for temperature monitoring and control in precision agriculture.

CRediT authorship contribution statement

Ke Xu: Conceptualization, Methodology, Software, Experiment, Formal analysis, Writing – original draft, Writing – review & editing. **Xuan Guo:** Methodology, Software, Writing – review & editing. **Junming He:** Experiment, Formal analysis, Writing – review & editing. **Bin Yu:** Experiment, Formal analysis, Writing – review & editing. **Jinglu Tan:** Formal analysis, Writing – review & editing. **Ya Guo:** Conceptualization, Methodology, Formal analysis, Writing – review & editing, Supervision, Project administration, Funding acquisition.

Declaration of Competing Interest

The authors declare that they have no known competing financial interests or personal relationships that could have appeared to influence the work reported in this paper.

Acknowledgements

This work was supported in part by National Natural Science Foundation of China (No: 51961125102, No: 31771680), Wuxi Science and Technology Development Funding (N20203012) and the 111 Project (B12018).

Appendix A. ASHRAE solar radiation model

$$R_{dir} = R_{dn}cos\theta \tag{A1}$$

$$R_{dn} = R_{d0}e^{-K_a/sinh} \tag{A2}$$

$$K_a = 0.174 + 0.035sin\left(\frac{2\pi(d-100)}{365}\right) \tag{A3}$$

$$R_{d0} = 1160 + 75sin\left(\frac{2\pi(d-275)}{365}\right) \tag{A4}$$

$$sinh = sin\varphi sin\delta + cos\varphi cos\delta cos\tau \tag{A5}$$

$$\delta = 23.45^{\circ} \times sin\left(\frac{2\pi(d+284)}{365}\right) \tag{A6}$$

$$\tau = (12-t) \times 15^{\circ} \tag{A7}$$

Here R_{dir} is the direct solar radiation in any plane, R_{dn} is the direct solar normal radiation reaching the ground in nature, θ is the angle between the direct solar radiation and the normal line of any wall, R_{d0} is the direct solar radiation of the upper boundary of the atmosphere, h is the solar altitude angle, K_a is the atmospheric optical extinction coefficient, d is the cumulative day from January 1, φ is the geographical latitude, where the northern latitude is positive, the southern latitude is negative, δ is the angle of declination, τ is the time angle, t is the local time.

$$R_{dif}^{v} = K_{sd}YR_{dn} \tag{A8}$$

$$R_{dif}^{nv} = K_{sd}R_{dn}\frac{(1+cos\theta_{sh})}{2} \tag{A9}$$

R_{dif}^{v} is the diffuse solar radiation on the vertical part of the radiated surface, R_{dif}^{nv} is the diffuse solar radiation on the non-vertical surface, K_{sd} is the constant ratio of the scattered radiation from the plane to the normal incident direct radiation (ASHRAE Handbook of Fundamentals), Y is the ratio of the diffuse radiation on the vertical surface to the diffuse radiation from the sky on the horizontal surface, and θ_{sh} is the ratio between the surface and the horizontal surface and θ_{sh} is the inclination angle between the surface and the horizontal.

Appendix B:. *k-ε* turbulence model

$$\frac{\partial(\rho k)}{\partial t} + \frac{\partial(\rho k u_i)}{\partial x_i} = \frac{\partial}{\partial x_j}\left[\left(\mu + \frac{\mu_t}{\sigma_k}\right)\frac{\partial k}{\partial x_j}\right] + G_k + G_b - \rho\varepsilon \tag{B1}$$

$$\frac{\partial(\rho\varepsilon)}{\partial t} + \frac{\partial(\rho\varepsilon u_i)}{\partial x_i} = \frac{\partial}{\partial x_j}\left[\left(\mu + \frac{\mu_t}{\sigma_\varepsilon}\right)\frac{\partial \varepsilon}{\partial x_i}\right] + C_{1\varepsilon}\frac{\varepsilon}{k}(G_k + C_{3\varepsilon}G_b) - C_{2\varepsilon}\rho\frac{\varepsilon^2}{k} \tag{B2}$$

Here k is the turbulent kinetic energy, ε is the dissipation velocity, ρ is the density, u is the velocity, x_i and x_j are the directional length component. The other variables are expressed as:

$$\mu_t = \rho C_\mu \frac{k^2}{\varepsilon} \tag{B3}$$

$$G_k = \mu_t S^2 \tag{B4}$$

$$G_b = \beta g_i \frac{\mu_t}{Pr_t} \frac{\partial T}{\partial x_i} \tag{B5}$$

$$\beta = -\frac{1}{\rho}\left(\frac{\partial \rho}{\partial T}\right)_p \tag{B6}$$

Here μ_t is turbulent viscosity, G_k is turbulent kinetic energy generated by laminar velocity gradient, S is the average strain tensor, G_b is turbulent kinetic energy generated by buoyancy, β is thermal expansion coefficient, P_{rt} is turbulent Prandt number of energies, and its default value is 0.85, g_i is gravity vector component. Other constants $C_{1\varepsilon} = 1.44$, $C_{2\varepsilon} = 1.92$, $C_\mu = 0.09$, $\sigma_k = 1.0$, $\sigma = 1.3$, where σ_k and σ_ε are the Prandt number of turbulent kinetic energy and turbulent dissipation rate respectively.

Appendix C:. The vertical view of greenhouse temperature comparison

It can be seen by the comparison of the top view (Figs. C1 and C2) that at 9:00 and 15:00, the temperature difference between the east and west sides of the greenhouse is obvious, which is due to the change of solar radiation direction. In the morning and afternoon, the side that receives direct sunlight is about 5 °C higher than the side that does not, and this difference is about 3 °C less without considering the crop effects. In the greenhouse with considering crops, the air temperature above the uncovered soil reached 41 °C, and the temperature at the south side of the greenhouse is about 5 °C higher than that at the north side. The temperature without considering the crop effects is about 2 °C–3 °C higher than the temperature with considering crop area.

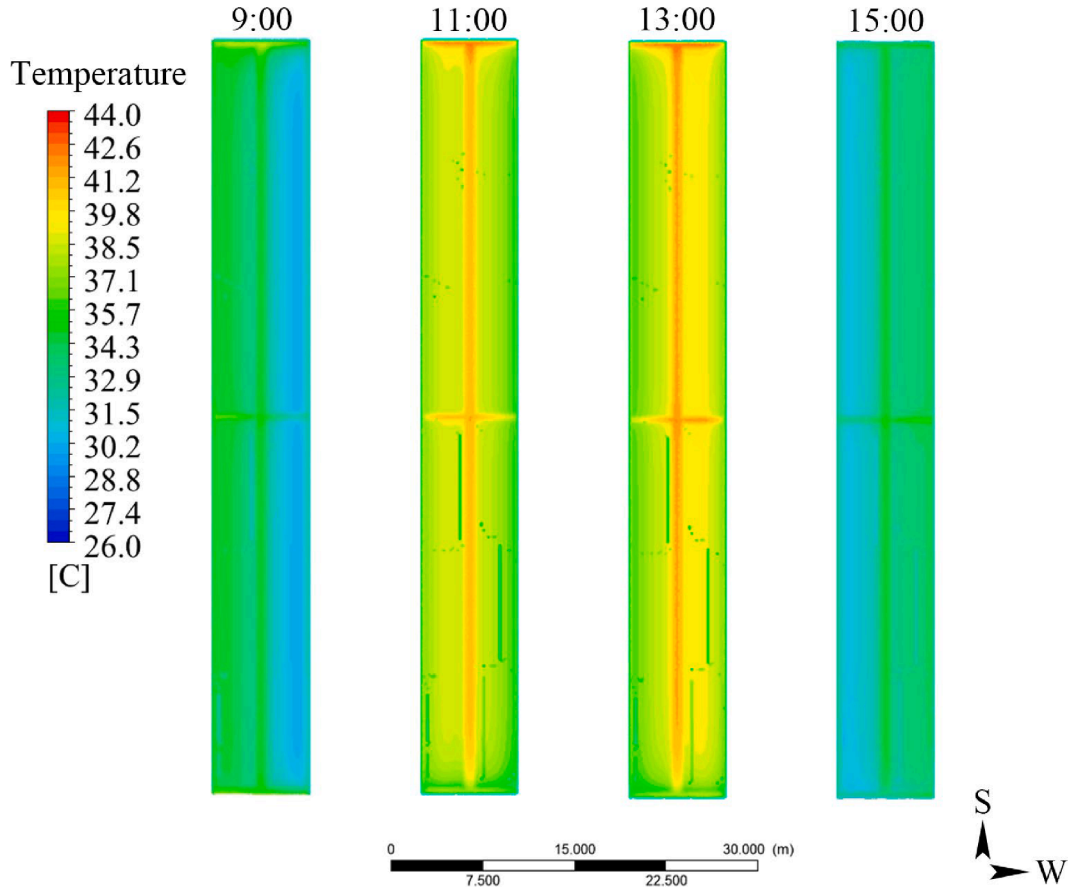

Fig. C1. Illustration of temperature distribution on a horizontal plane at the height of 1 m in the greenhouse with considering crop.

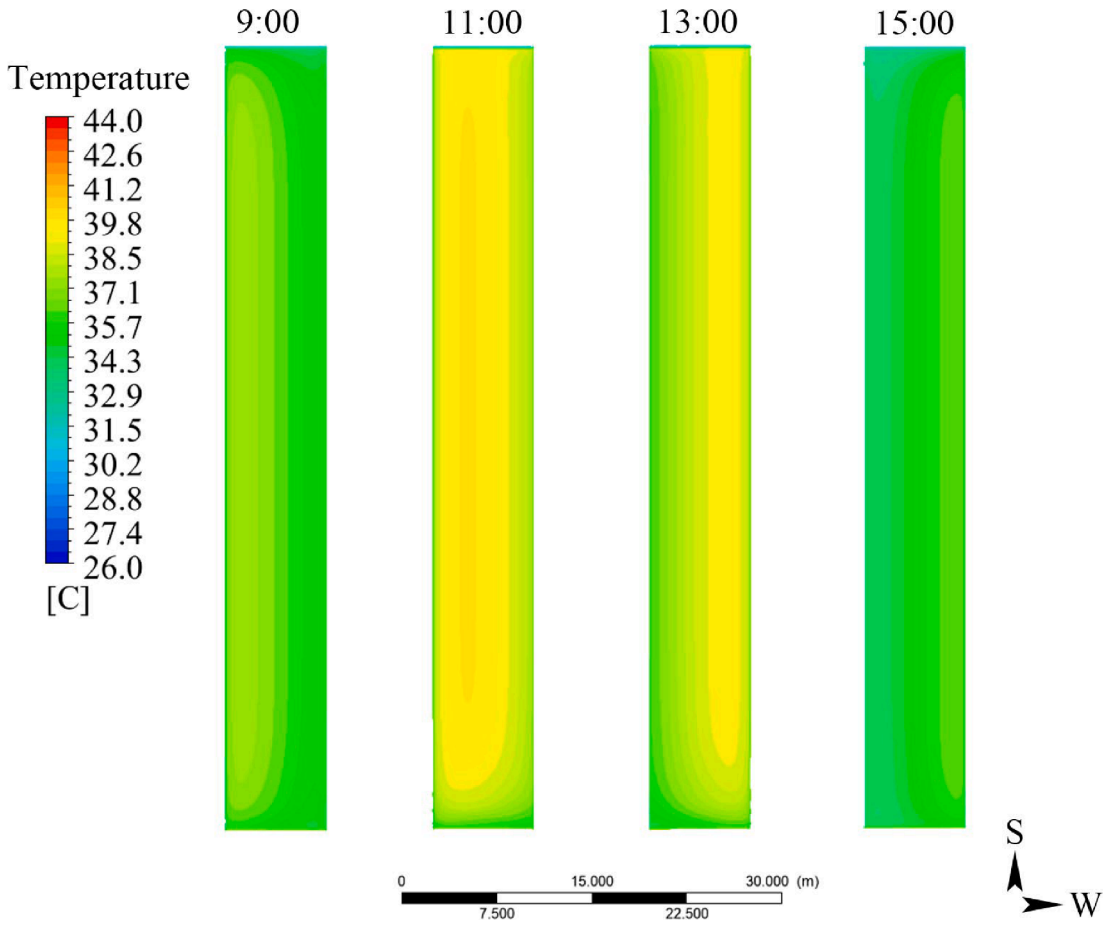

Fig. C2. Illustration of temperature distribution on a horizontal plane at the height of 1 m in the greenhouse without considering crop.

References

[1] Lin D, Zhang L, Xia X. Hierarchical model predictive control of Venlo-type greenhouse climate for improving energy efficiency and reducing operating cost. J Clean Prod 2020;264:121513. https://doi.org/10.1016/j.jclepro.2020.121513.

[2] Mahdavi S, Sarhaddi F, Hedayatizadeh M. Energy/exergy based-evaluation of heating/cooling potential of PV/T and earth-air heat exchanger integration into a solar greenhouse. Appl Therm Eng 2019;149:996–1007. https://doi.org/10.1016/j.applthermaleng.2018.12.109.

[3] Dhiman M, Sethi VP, Singh B, Sharma A. CFD analysis of greenhouse heating using flue gas and hot water heat sink pipe networks. Comput Electron Agric 2019;163:104853. https://doi.org/10.1016/j.compag.2019.104853.

[4] Entezari A, Wang RZ, Zhao S, Mahdinia E, Wang JY, Tu YD, et al. Sustainable agriculture for water-stressed regions by air-water-energy management. Energy 2019;181:1121–8. https://doi.org/10.1016/j.energy.2019.06.045.

[5] Choab N, Allouhi A, Maakoul AE, Kousksou T, Saadeddine S, Jamil A. Review on greenhouse microclimate and application: Design parameters, thermal modeling and simulation, climate controlling technologies. Sol Energy 2019;191:109–37. https://doi.org/10.1016/j.solener.2019.08.042.

[6] Cao K, Xu H, Zhang R, Xu D, Yan L, Sun Y, et al. Renewable and sustainable strategies for improving the thermal environment of Chinese solar greenhouses. Energy Build 2019;202:109414. https://doi.org/10.1016/j.enbuild.2019.109414.

[7] Boulard T, Roy JC, Pouillard JB, Fatnassi H, Grisey A. Modelling of micrometeorology, canopy transpiration and photosynthesis in a closed greenhouse using computational fluid dynamics. Biosyst Eng 2017;158:110–33. https://doi.org/10.1016/j.biosystemseng.2017.04.001.

[8] Mazzeo D, Baglivo C, Panico S, Congedo PM. Solar greenhouses: Climates, glass selection, and plant well-being. Sol Energy 2021;230:222–41. https://doi.org/10.1016/j.solener.2021.10.031.

[9] Hassanien RHE, Li M, Lin W. Advanced applications of solar energy in agricultural greenhouses. Renew Sustain Energy Rev 2016;54:989–1001. https://doi.org/10.1016/j.rser.2015.10.095.

[10] Zhang G, Ding X, Li T, Pu W, Lou W, Hou J. Dynamic energy balance model of a glass greenhouse: An experimental validation and solar energy analysis. Energy 2020;198:117281. https://doi.org/10.1016/j.energy.2020.117281.

[11] Van Beveren PJM, Bontsema J, Van Straten G, Van Henten EJ. Optimal control of greenhouse climate using minimal energy and grower defined bounds. Appl Energy 2015;159:509–19. https://doi.org/10.1016/j.apenergy.2015.09.012.

[12] Mobtaker HG, Ajabshirchi Y, Ranjbar SF, Matloobi M. Simulation of thermal performance of solar greenhouse in north-west of Iran: An experimental validation. Renewable Energy 2019;135:88–97. https://doi.org/10.1016/j.renene.2018.10.003.

[13] Berroug F, Lakhal EK, El Omari M, Faraji M, El Qarnia H. Thermal performance of a greenhouse with a phase change material north wall. Energy Build 2011;43(11):3027–35. https://doi.org/10.1016/j.enbuild.2011.07.020.

[14] Bonuso S, Panico S, Baglivo C, Mazzeo D, Matera N, Congedo PM, et al. Dynamic Analysis of the Natural and Mechanical Ventilation of a Solar Greenhouse by Coupling Controlled Mechanical Ventilation (CMV) with an Earth-to-Air Heat Exchanger (EAHX). Energies 2020;13(14):3676. https://doi.org/10.3390/en13143676.

[15] Nebbali R, Roy JC, Boulard T. Dynamic simulation of the distributed radiative and convective climate within a cropped greenhouse. Renewable Energy 2012;43:111–29. https://doi.org/10.1016/j.renene.2011.12.003.

[16] Fidaros DK, Baxevanou CA, Bartzanas T, Kittas C. Numerical simulation of thermal behavior of a ventilated arc greenhouse during a solar day. Renewable Energy 2010;35(7):1380–6. https://doi.org/10.1016/j.renene.2009.11.013.

[17] Baglivo C, Mazzeo D, Panico S, Bonuso S, Matera N, Congedo PM, et al. Complete greenhouse dynamic simulation tool to assess the crop thermal well-being and energy needs. Appl Therm Eng 2020;179:115698. https://doi.org/10.1016/j.applthermaleng.2020.115698.

[18] Reyes-Rosas A, Molina-Aiz FD, Valera DL, López A, Khamkure S. Development of a single energy balance model for prediction of temperatures inside a naturally ventilated greenhouse with polypropylene soil mulch. Comput Electron Agric 2017;142:9–28. https://doi.org/10.1016/j.compag.2017.08.020.

[19] Serageldin AA, Abdelrahman AK, Ookawara S. Earth-Air Heat Exchanger thermal performance in Egyptian conditions: Experimental results, mathematical model, and Computational Fluid Dynamics simulation. Energy Convers Manage 2016;122:25–38. https://doi.org/10.1016/j.enconman.2016.05.053.

[20] Norton T, Sun D-W, Grant J, Fallon R, Dodd V. Applications of computational fluid dynamics (CFD) in the modelling and design of ventilation systems in the agricultural industry: a review. Bioresour Technol 2007;98(12):2386–414. https://doi.org/10.1016/j.biortech.2006.11.025.

[21] Tong G, Christopher DM, Zhang G. New insights on span selection for Chinese solar greenhouses using CFD analyses. Comput Electron Agric 2018;149:3–15. https://doi.org/10.1016/j.compag.2017.09.031.

[22] Saberian A, Sajadiye SM. The effect of dynamic solar heat load on the greenhouse microclimate using CFD simulation. Renewable Energy 2019;138:722–37. https://doi.org/10.1016/j.renene.2019.01.108.
[23] Zhang G, Fu Z, Yang M, Liu X, Dong Y, Li X. Nonlinear simulation for coupling modeling of air humidity and vent opening in Chinese solar greenhouse based on CFD. Comput Electron Agric 2019;162:337–47. https://doi.org/10.1016/j.compag.2019.04.024.
[24] Huang S, Yan H, Zhang C, Wang G, Acquah SJ, Yu J, et al. Modeling evapotranspiration for cucumber plants based on the Shuttleworth-Wallace model in a Venlo-type greenhouse. Agric Water Manage 2020;228:105861. https://doi.org/10.1016/j.agwat.2019.105861.
[25] Yao W, Xu C, Zhao J, Wang X, Wang Y, Li X, et al. The modified ASHRAE model based on the mechanism of multi-parameter coupling. Energy Convers Manage 2020;209:112642. https://doi.org/10.1016/j.enconman.2020.112642.
[26] Shklyar A, Arbel A. Numerical model of the three-dimensional isothermal flow patterns and mass fluxes in a pitched-roof greenhouse. J Wind Eng Ind Aerodyn 2004;92(12):1039–59. https://doi.org/10.1016/j.jweia.2004.05.008.
[27] Ahmed SF, Amanullah MTO, Khan MMK, Rasul MG, Hassan NMS. Parametric study on thermal performance of horizontal earth pipe cooling system in summer. Energy Convers Manage 2016;114:324–37. https://doi.org/10.1016/j.enconman.2016.01.061.
[28] Baneshi M, Gonome H, Maruyama S. Wide-range spectral measurement of radiative properties of commercial greenhouse covering plastics and their impacts into the energy management in a greenhouse. Energy 2020;210:118535. https://doi.org/10.1016/j.energy.2020.118535.
[29] Cheng X, Li D, Shao L, Ren Z. A virtual sensor simulation system of a flower greenhouse coupled with a new temperature microclimate model using three-dimensional CFD. Comput Electron Agric 2021;181:105934. https://doi.org/10.1016/j.compag.2020.105934.
[30] Yan H, Acquah SJ, Zhang C, Wang G, Huang S, Zhang H, et al. Energy partitioning of greenhouse cucumber based on the application of Penman-Monteith and Bulk Transfer models. Agric Water Manage 2019;217:201–11. https://doi.org/10.1016/j.agwat.2019.02.036.